Transition Modeling based on the Dual N-factor Method for the CRM-NLF Wind Tunnel Configuration

Pedro Paredes,* Balaji Venkatachari,†
National Institute of Aerospace, Hampton, VA 23666, USA

Meelan M. Choudhari,‡ Fei Li §
NASA Langley Research Center, Hampton, VA 23681, USA

The dual N-factor method is used to model the boundary-layer transition over the common research model with natural laminar flow (CRM-NLF) aircraft configuration. The flow conditions match selected test conditions from a wind tunnel experiment in the National Transonic Facility at the NASA Langley Research Center. The paper presents a systematic methodology for transition prediction in the presence of a dual shock system and extends the prior capability for iteratively coupled computational fluid dynamics (CFD) predictions to incorporate three-dimensional, transonic wings. The method employs stability computations based on the linear parabolized stability equations (PSE), along with a dual N-factor criterion. The iterative process begins with the fully turbulent Reynolds-averaged-Navier-Stokes (RANS) mean flow solution. For the first iteration, a mean flow solution is calculated with an imposed transition front that aligns with the shock front from the fully turbulent solution. Subsequently, stability computations are performed along a set of streamlines across the wing to calculate the amplification of planar Tollmien-Schlichting (TS) and stationary crossflow (CF) modes. The transition criterion based on the dual N-factor method is used to infer the updated transition front and the process is successively repeated until convergence of the solution. Within three iterations, the predicted fronts for angles of attack of 1.45, 1.98, 2.46 and 2.94 degrees and a mean-aerodynamic-chord Reynolds number equal to 15 million, approach visual convergence in most regions of the studied cases, and the resulting predictions are in good agreement with the transition fronts deduced from measurements of temperature-sensitive paint. Even though surface pressure measurements based on fully-turbulent flow agree well with the measured pressure coefficient distributions, strong viscous-inviscid interaction effects cause significant shifts in the shock locations based on the imposed transition front, underscoring the intrusive nature of static pressure measurements using surface mounted ports on the CRM-NLF configuration.

Nomenclature

AoA	=	angle of attack [deg]
C_p	=	surface pressure coefficient
f	=	disturbance frequency [Hz]
L	=	reference length [m]
M	=	Mach number
MAC	=	mean aerodynamic chord [m]
N	=	logarithmic amplification factor
$\bar{\mathbf{q}}$	=	vector of base flow variables
$\tilde{\mathbf{q}}$	=	vector of perturbation variables
$\hat{\mathbf{q}}$	=	vector of amplitude variables
Re_{MAC}	=	Reynolds number based on MAC

*Senior Research Engineer, Computational AeroSciences Branch, NASA LaRC. AIAA Senior Member
†Senior Research Engineer, Computational AeroSciences Branch, NASA LaRC. AIAA Senior Member
‡Research Scientist, Computational AeroSciences Branch. AIAA Fellow
§Research Scientist, Computational AeroSciences Branch.

Re_∞	=	freestream unit Reynolds number [m^{-1}]
T	=	temperature [K]
(u, v, w)	=	streamwise, wall-normal, and spanwise velocity components [m s^{-1}]
(x, y, z)	=	Cartesian coordinates [m]
x/c	=	chordwise coordinate scaled by reference chord length
y^+	=	near wall grid spacing in wall units
α	=	streamwise wavenumber [m^{-1}]
β	=	spanwise wavenumber [m^{-1}]
λ	=	spanwise wavelength [m]
δ	=	boundary layer thickness [m]
ω	=	disturbance angular frequency [rad s^{-1}]
ρ	=	density [kg m^{-3}]
σ	=	spatial growth rate [m^{-1}]
(ξ, η, ζ)	=	streamwise, wall-normal, and spanwise coordinates [m]
Subscript		
∞	=	freestream value
c	=	critical value

I. Introduction

Substantial reductions in the fuel burn of future aircraft have been targeted both in the U.S. [1] and Europe [2] in order to lower the cost of air travel and to alleviate the impact of aviation on the environment. A significant fraction of the targeted reductions in aircraft fuel burn come from reductions in vehicle drag. For today's commercial transport aircraft, up to one half of the total drag corresponds to skin friction drag. Because laminar skin friction is much lower in comparison with turbulent skin friction, flow control via delayed boundary-layer transition over major aerodynamic surfaces holds the potential to provide the desired reductions in the overall drag.

According to the CFD Vision 2030 [3], the most critical areas in computational fluid dynamics (CFD) simulation capability that will remain a pacing item for the foreseeable future is the ability to adequately predict viscous flows with transition-to-turbulence and flow separation. A majority of CFD computations are carried out under the assumption that the flow is turbulent everywhere, allowing the use of the computationally efficient Reynolds-averaged Navier-Stokes (RANS)-based turbulence models throughout the flowfield. However, for several applications ranging from wings with natural laminar flow (NLF) technology, high-lift configurations, rotorcraft flows, and unmanned aerial vehicles, the strong assumption involving a fully turbulent flow can lead to significant errors in the prediction of relevant performance metrics. Furthermore, most of the RANS models are incapable of modeling the process of transition from laminar to turbulent flow because of the complexity involved in the physics of the transition onset process [4–6]. The inherent averaging process in the RANS procedure makes it difficult to capture the development of the linear disturbances that initiate the laminar-turbulent transition process within the initially laminar boundary layer as well as the subsequent nonlinear growth of those disturbances and the eventual breakdown to turbulence.

Semiempirical correlations based on linear stability theory (LST), such as the e^N method introduced by Smith and Gamberoni [7] and Ingen [8], remain widely used approaches for the prediction of transition onset locations in aircraft design computations. The LST equations are derived from the linearized Navier-Stokes equations to track the evolution of small amplitude, fixed frequency disturbances under the parallel flow assumption. The e^N method does require the specification of a critical N-factor that must be obtained from correlations against experimentally measured transition locations. Transition analysis using the parabolized stability equations (PSE) [9] involves less restrictive assumptions and can also account for the effects of a weakly nonparallel basic state, both streamwise and transverse curvatures in the surface geometry, and nonlinear modal interactions of the laminar instabilities. Both LST and PSE can account for the amplification of the dominant primary instabilities encountered on aircraft wings, namely, the Tollmien-Schlichting waves and the stationary and traveling crossflow vortices. However, the application of these approaches toward a coupled computation of laminar, transitional, and fully turbulent parts of a flowfield entails an increased computational cost as well as complexity; it also suffers from a lack of robustness and often requires adequate understanding of transition physics and hydrodynamic stability theory that typical users of CFD codes may not know. To alleviate or circumvent these shortcomings, surrogate models are often used in lieu of the direct computation of stability characteristics based on the laminar flow information provided by the flow solver. There are a number of successful implementations of CFD codes that combine stability-based transition predictions with RANS-based turbulence modeling [10–17].

The present research seeks to blend the so-called physics-based approach for transition modeling with the RANS-based approaches, with the eventual goal of developing a reliable and cost efficient, yet robust and user-friendly, approach for integrated modeling of laminar-turbulent transition. To help achieve that goal, this particular paper focuses on the assessment of an iterative procedure for transition modeling via linear stability correlations based on the parabolized stability equations (PSE) for a swept, tapered wing at transonic conditions. This assessment is facilitated by the transition data obtained on the NASA common research model with natural laminar flow (CRM-NLF) [18–20] that was tested in the National Transonic Facility.

On a typical transport aircraft wing with moderate sweep, transition occurs as a result of the crossflow (CF) instability and/or Tollmien-Schlichting (TS) instability, provided that the attachment line remains laminar. The CRM-NLF wing has been designed to modify the surface pressure distribution in such a way that the overall amplification of both of these instabilities is substantially reduced in comparison with that over a conventional wing. References [19, 21–24] have reported transition predictions based on stability correlations for TS and CF instabilities. However, those researchers applied classical linear stability theory (LST) that is considerably more robust than high-fidelity techniques such as the PSE, but also fails to account for the effects of surface curvature and mean-flow nonparallelism. Generally, aircraft wings tend to have purely convex curvature on the suction side, at least in the front portion of the wing surface where a laminar boundary layer flow may be expected. Convex curvature reduces the growth rates of crossflow instabilities, whereas the growth of the boundary layer along the chordwise direction tends to destabilize the crossflow modes. Thus, it is generally assumed that the two effects would offset each other, so that a low-fidelity stability prediction based on the classical, quasiparallel LST would provide accurate N-factor predictions. However, the validity of this assumption was brought into question by Malik et al. [25], who showed that the effects of surface curvature can be appreciable for NLF applications related to subsonic transports and that they may not always be balanced by the countereffects of a nonparallel mean flow. As a result, it is desirable to include these effects for the CRM-NLF. The PSE includes both of these effects and its initial application to the CRM-NLF configuration was described in previous papers [26, 27]; however, the transition front was imposed at the measured location for the calculation of the mean flow solutions.

While results from Paredes et al. [26] and Venkatachari et al. [27] showed that the measured transition front was approximately consistent with that obtained using a dual N-factor criterion, a priori knowledge of the transition front is not available during CFD predictions in a typical design context. Furthermore, these analyses suggest that the complex flowfield over the CRM-NLF configurations entails a strong coupling between the transition front and the shocks on the suction surface and that pockets of flow separation may appear depending on the relative locations of the shocks. Thus, an iterative approach is necessary to make accurate predictions of aerodynamic drag over the wing. The present paper seeks to extend the previous state-of-the-art by combining PSE-based stability predictions with an iterative solution procedure for the CRM-NLF configuration. Applications of this approach to cannonical flow configurations have been described in Refs. [28–31]; however, the configurations addressed in those papers were significantly simpler than the CRM-NLF. The present study is the first attempt to use an iterative strategy based on PSE in the case of a realistic, transport-related configuration with multiple, disjoint shocks.

The paper is organized as follows. §II provides a summary of the linear stability formulation used in this paper. The mean flow solutions and instability results for the selected CRM-NLF configuration are presented in §III. Finally, a summary of the present results are presented in §IV.

II. Transition Prediction Methodology

This section introduces the methodology used in this paper for transition prediction over the wing of the CRM-NLF at selected conditions from wind tunnel experiments in the National Transonic Facility at the NASA Langley Research Center [18–20].

A. Linear Stability Analysis

The stability characteristics of the three-dimensional boundary layer over the CRM-NLF configurations is studied with a nonorthogonal curvilinear coordinate system as implemented in the LASTRAC.3d code [32]. The nonorthogonal curvilinear coordinate system allows the selection of the streamwise direction (ξ) to be along the streamline, while the spanwise direction (ζ) is selected to be along the spanwise surface grid lines that run parallel to the leading and trailing edges. The remaining coordinate is defined in the wall normal direction (η). Results for boundary layers over infinite-swept-wing configurations have been shown to be identical between the orthogonal and nonorthogonal coordinate systems [32].

The parabolized stability equations (PSE) are used to calculate the amplification of boundary-layer instability waves

along a set of streamlines over the selected configurations. The PSE approach accounts for the effects of the streamwise curvature and streamwise gradients of the mean flow and instability variables. The perturbations have the form

$$\tilde{\mathbf{q}}(\xi,\eta,\zeta,t) = \hat{\mathbf{q}}(\xi,\eta)\exp\left[\mathrm{i}\left(\int_{\xi_0}^{\xi}\alpha(\xi')\,\mathrm{d}\xi' + \beta\zeta - \omega t\right)\right], \tag{1}$$

where the unknown, streamwise varying wavenumber $\alpha(\xi)$ is determined in the course of the solution by imposing the normalization condition to ensure a slow variation of the amplitude functions $\hat{\mathbf{q}}(\xi,\eta,\zeta) = (\hat{\rho},\hat{u},\hat{v},\hat{w},\hat{T})^T$ in the streamwise direction in comparison with the phase term $\exp\left[\mathrm{i}\int_{\xi_0}^{\xi}\alpha(\xi')\,\mathrm{d}\xi'\right]$. The PSE are obtained by substituting Eq. (1) into the linearized Navier-Stokes equations and incorporating the scale separation to neglect the viscous, streamwise derivative terms, A more detailed description of the method can be found in Refs. [9, 32, 33].

The nonparallel growth rate of the disturbance with a selected combination of ω and β is defined as

$$\sigma(\xi,\omega,\beta) = -\Im(\alpha) + \frac{1}{2}\frac{\mathrm{d}K}{\mathrm{d}\xi}, \tag{2}$$

and is based on the disturbance kinetic energy norm K.

The onset of laminar-turbulent transition is estimated using the logarithmic amplification ratio, the so-called N-factor, relative to the neutral location ξ_I where the disturbance first becomes unstable,

$$N(\xi,\omega,\beta) = -\int_{\xi_I}^{\xi}\sigma(\xi',\omega,\beta)\,\mathrm{d}\xi'. \tag{3}$$

Here, we assume that transition onset is likely to occur when a function of N-factor envelope values based on stationary crossflow instability waves, N_{CF}, and based on traveling Tollmien-Schlichting instability waves, N_{TS}, reaches a certain threshold [34–36]. The expression of the dual $N_{TS} - N_{CF}$ criterion can be written as

$$\mathcal{I}(N_{TS},N_{CF}) \equiv \left(\frac{N_{TS}}{N_{TS,c}}\right)^{a_{TS}} + \left(\frac{N_{CF}}{N_{CF,c}}\right)^{a_{CF}} = 1, \tag{4}$$

where the subscript c refers to the critical value, and the exponents a_{TS} and a_{CF} control the level of interaction between the two types of instability waves. For the present calculations, $N_{TS,c} = N_{CF,c} = 6$ and $a_{TS} = a_{CF} = 3$ as discussed by Paredes et al. [26] for the configurations I and II with imposed front at the measured location. The critical $N_{TS,c} = 6$ is selected based on the turbulence level of the NTF estimated by Crouch et al. [37] to be 0.24% and confirmed by the direct measurements taken by King et al. [38]. The remaining parameters were calibrated by Paredes et al. [26] for selected CRM-NLF configurations with imposed transition fronts at the measured locations.

B. Iterative Method for Transition Modeling

An iterative method is proposed to predict and model the transitional boundary layer over the selected CRM-NLF configurations. As explained by Paredes et al. [26], the viscous-inviscid interactions lead to a downstream movement of the shock fronts along the suction surface for the transitional flow with an imposed transition (IT) front at the measured location in comparison with the fully-turbulent (FT) flow solution (i.e., without enforcing laminar regions or fixing transition). Therefore, an iterative process is needed for arriving at the converged transition front and mean flow solution. Furthermore, Paredes et al. [26] observed that the measured transition fronts were close to the shocks in the outboard regions of the wing, which would indicate that the presence of the shock can have an important influence on the transition process. Based on these observations, an iterative method is proposed following these steps:

1) Calculate FT mean flow and extract the shock front.
2) Calculate mean flow with IT front set to the shock front from the FT solution and extract the new shock front.
3) Perform stability analysis along streamlines up to the IT front. Define a new transition front by taking the point on each streamline where (a) the dual N-factor reaches unity or (b) the shock front is reached (if transition is not predicted upstream of the IT front).
4) Calculate mean flow with the new predicted transition front and extract the shock front.

The last two steps are repeated until the desired convergence criterion has been met. The extraction of the shock front is based on the Jameson shock sensor [39], which is essentially a normalized second difference of the pressure. The sensor implementation follows along the process outlined in Ref. [40]. The shock location is determined to be the

location where the shock sensor along a streamwise grid line reaches its maximum, such that when multiple shocks are encountered, the front is selected at the stronger shock. Alternatively, the downstream shock is selected in situations where two shocks of similar strength are observed. The choice of where to shift form one shock to another shock is justified a posteriory by the comparison with the experimental data, but may need to be revised for other cases.

The predicted front is calculated along each streamline as the location where the dual N-factor criterion is reached upstream of the imposed transition front or is otherwise set at the shock front. However, due to the upstream influence of the transition onset on the laminar solution, extrapolation of the N-factor values is used to find out if the criterion is met within the vicinity of the imposed front. The predicted transition front is updated with an underrelaxation of 0.75 to help reach convergence. The predicted front is also smoothed via a three-point stencil average.

We note that similarly strong viscous-inviscid interactions also occur in low-speed airfoils with separation bubble(s), where transition onset has a strong effect on the inviscid pressure distribution and the extent of the separation bubble. This was modeled via an iterative process with underrelaxation [29, 30]. In particular, it was shown that the iterative procedure was robust enough to converge, irrespective of whether the initial guess for transition location was upstream or downstream of the separation location in the final solution.

III. Results

This section begins with a brief overview of the CRM-NLF configuration. Following that, the mean flow solutions at the selected flow conditions are presented. Then, the TS and CF amplification at those conditions are analyzed with the PSE formulation for the suction side alone. Finally, the predicted transition locations based on the dual N-factor method are compared with the measured transition fronts on the suction side of the wing as reported by Lynde et al. [19].

A. CRM-NLF

The CRM is an open geometry representation of a generic transport vehicle and has been used in a multitude of studies [41]. The CRM-NLF builds upon this geometry by replacing the wing with a new one that supports NLF on the upper surface of the wing. The outer mold line (OML) of the CRM-NLF wing was defined using the Constrained Direct Iterative Surface Curvature (CDISC) NLF design method [42]. The wind-tunnel model is a 5.2% scaled semispan model of the CRM-NLF. The model has a semispan length of 1.5278 m, mean aerodynamic chord of 0.36383 m, and a leading-edge sweep of 37.3° outboard of the break, which is gradually reduced to 12.9° over the inboard 10% of the wing. Further details on the CRM-NLF geometry can be found in Ref. [21] and on the CRM webpage (`https://commonresearchmodel.larc.nasa.gov/crm-nlf`).

The experiments were conducted in the National Transonic Facility (NTF) [18–20]. The effective turbulence level of the NTF was estimated by Crouch et al. [37] to be 0.24% based on the variable N-factor correlation proposed by Mack [43] with a critical $N_{TS} = 6$. The surface roughness of the model was specified to be 2.28×10^{-5} mm [18]. The approximated transition fronts were extracted from the Temperature Sensitive Paint (TSP) images by Lynde et al. [18, 19].

B. Mean Flow Solutions

The mean flow is computed by using the NASA OVERFLOW 2.3b solver [44]. OVERFLOW is a Navier-Stokes solver for structured, overset grids that is capable of computing both time-accurate and steady-state solutions via a variety of options for spatial and temporal discretizations. The CRM-NLF computations are run at four flow conditions that are detailed in Table 1. These flow conditions correspond to the problem statement specified by the AIAA Transition Modeling and Prediction workshop organizers (`https://transitionmodeling.larc.nasa.gov/wp-content/uploads/sites/109/2020/02/TransitionMPW_CaseDescriptions.pdf`). Solutions with FT flow or transitional flow with an IT front are obtained using the Spalart-Allmaras (SA) RANS model [45]. In the IT front solutions, the boundary layer remains laminar until the specified location of transition. For the pressure side, the transition front is imposed roughly at the 5% chord location, to be consistent with the manner in which the suction side was tripped in the experiment. The mean flow solutions are obtained by running the flow solver in a steady-state manner by using the 3$^{\text{rd}}$-order Roe upwind scheme [46] and the unfactored successive symmetric overrelaxation (SSOR) implicit solution algorithm [47]. The computational grid has six overset near-body blocks (three on the fuselage, one wing-body collar grid, and two on the wing, including its tip). The generation of off-body grids and hole-cutting is performed with the OVERFLOW domain connectivity function (DCF). The grid has a near-wall spacing of $y^+ \approx 0.5$ and has approximately 40 wall-normal nodes along the boundary layer thickness and, 651 nodes around the wing in the

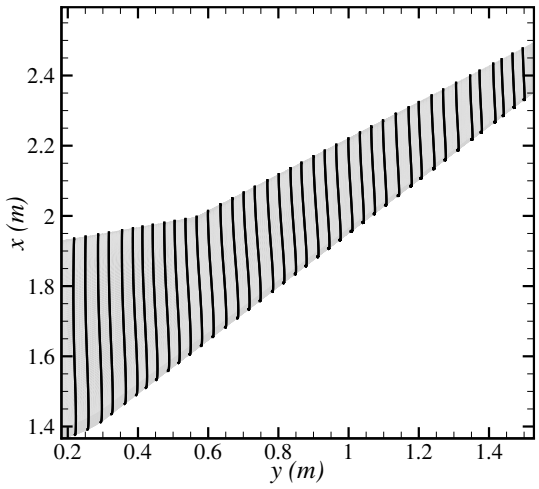


Fig. 1 Streamlines used for linear stability analysis over the wing of the CRM-NLF model for the third iteration of configuration I.

chordwise direction, and 401 nodes in the spanwise direction in the near-body grids. The total number of grid cells is 120 million. Further details of the grid are given by Venkatachari et al. [48].

Table 1 Flow conditions of selected configurations.

Configuration	AoA (°)	Re_{MAC} (10^6)	M_∞	$\bar{T}_\infty$ (K)	Re_∞ (10^6 m^{-1})
I	1.448	14.84	0.856	241.7	40.73
II	1.980	14.81	0.856	242.0	40.66
III	2.461	14.78	0.856	242.0	40.56
IV	2.937	14.72	0.856	243.0	40.41

C. Transition Modeling

The performance of the iterative procedure to calculate the transitional mean flow solutions over the CRM-NLF configurations of Table 1 is evaluated next. All results presented in this paper are based on three iterations of the CFD-stability integration.

The stability analysis is performed from the attachment line up to the imposed transition front location for a set of 40 streamlines across the wingspan as indicated in Fig. 1. The NASA LASTRAC.3d (nonorthogonal coordinate system) module of the LASTRAC solver [32, 33] is used to calculate the instability characteristics by using the PSE formulation.

The N-factor envelope results computed along the streamlines with PSE are discussed for the solutions corresponding to the first and third iterations of configuration I ($AoA = 1.45°$). Figures 2(a,c) and 2(b,d) show the contours of N_{CF} and N_{TS}, respectively, within the laminar region of each iteration. High N_{CF} values larger than 6 are found in a narrow region just inboard of the break, as well as in the midspan region of the wing from $y = 0.65$ m to 0.85 m, and in the outboard region of the wing for $y > 1.1$ m. The N_{TS} contours of Fig. 2(b) show how the $N_{TS} \approx 7$ isoline aligns with the experimental transition front in the inboard region of the wing within the range of $y \in [0.3, 0.55]$ m. The value of N_{TS} decreases at farther outboard stations (i.e., larger values of y), where the transition front is approximately aligned with the second (i.e., aft) shock. For the first iteration, a laminar separation bubble induced by the inboard shock is found from $y = 0.95$ m to 1.1 m outboard of the shift in the imposed front from the upstream shock to the downstream shock. However, the high levels of N_{TS} and N_{CF} within this region leads to a predicted front that agrees with the measured front and corrects the location of the shift of the imposed front between the shocks. A local peak of N_{TS} is also present near $y = 1.1$ m for the third iteration as shown in Fig. 2(d). A small separation region is still present due to the smoothing of the imposed transition front, and the effect on the overall solution is being investigated. The N_{TS} and

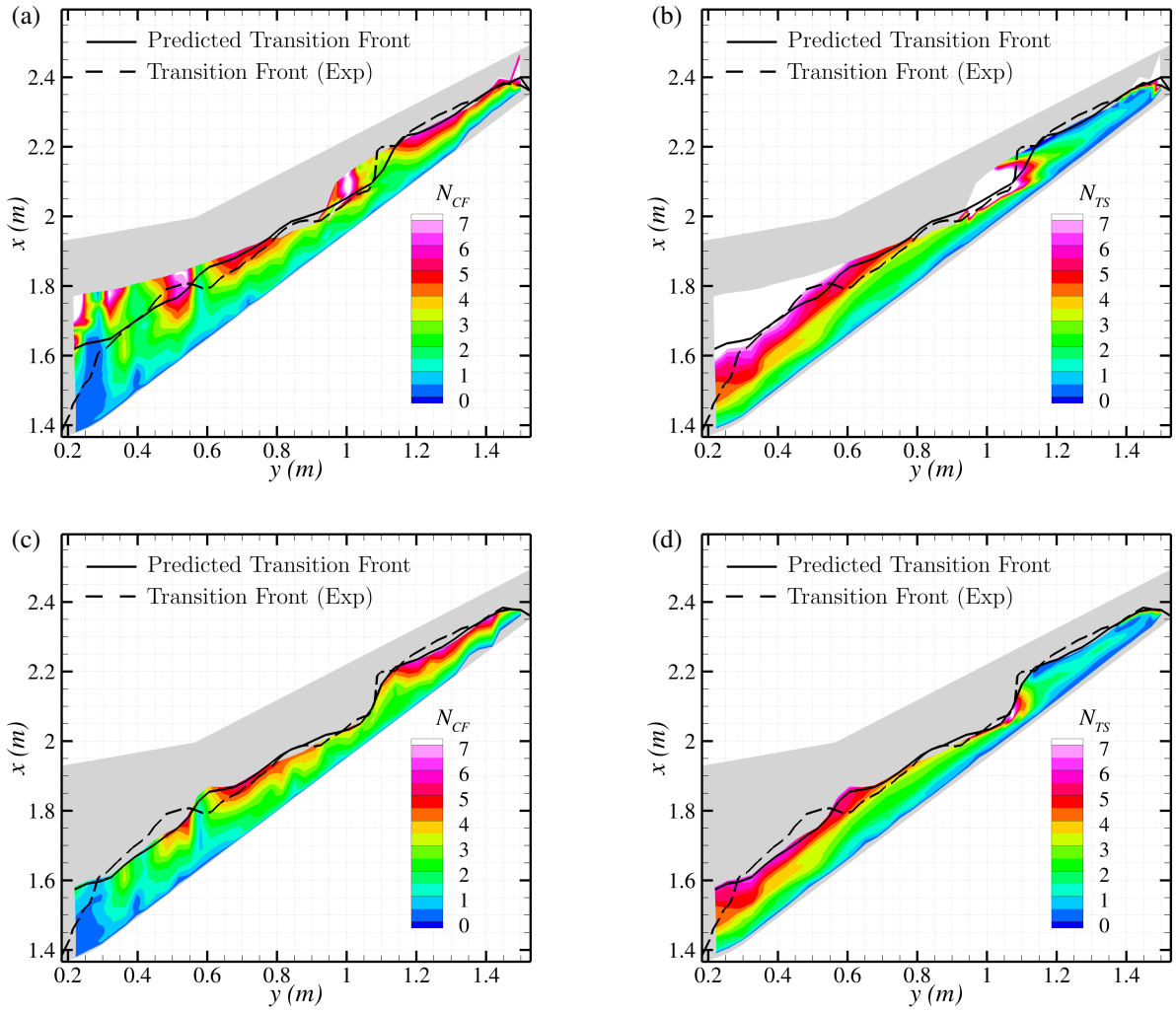


Fig. 2 N**-factor contours of (a,c) stationary CF waves (**$f = 0$**) and (b,d) TS waves (**$\beta = 0$**) for iterations (a,b) 1 and (c,d) 3 of configuration I (**$AoA = 1.45°$**).**

N_{CF} values only change slightly from iteration 1 to iteration 3 over the laminar region, which favor the need for few iterations to reach convergence of the predicted transition front.

The contours of the dual N-factor indicator function, $\mathcal{I}(N_{TS}, N_{CF})$, of Eq. (4) is shown in Fig. 3 for the third iteration of the configurations I and III detailed in Table 1. Similar results were obtained for the configurations II and IV. The approximate locations of the shocks for the FT and IT solutions are also shown. A downstream shift of the shocks is found for the configuration I between the FT and IT solutions (Fig. 3(a)). For the configuration III, the dual shock system found in the FT solution becomes a single shock in the IT solution. The changes in the shock locations yield leading order changes in pressure coefficient distribution that can affect the instability characteristics of the boundary layer.

Figures 4(a), 4(b), 4(c), and 4(d) show the TSP images and transition fronts extracted by Lynde et al. [19], the shock front from the FT solution used as the initial imposed front, and the predicted fronts for the conducted three iterations for the selected four angles of attack. As explained in Subsection II.B, the predicted transition front is formed by the locations along the selected streamlines where the critical value of the dual N-factor method defined by Eq. (4) is met or at the shock location when the criterion is not reached. The predicted fronts corresponding to iterations 2 and 3 are visually equivalent in most regions of the wing for the four cases. The small variations in some span regions indicate that additional iterations are required to reach convergence. Generally, the predicted transition fronts show an acceptable agreement with the experimental fronts. However, some uncertainty in the measured fronts extracted by Ref. [19] is

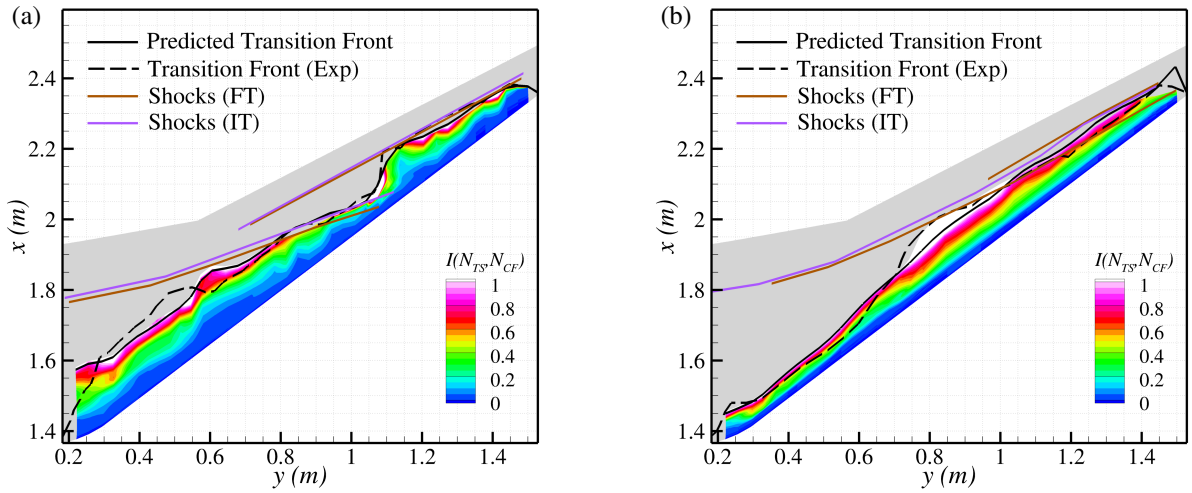


Fig. 3 Dual N-factor function contours for iteration 3 of configurations (a) I (AoA = 1.45°), and (b) III (AoA = 2.46°). The measured transition and the predicted transition front are shown with dashed and solid lines, respectively. The approximate locations of the shocks in the FT and IT solutions are also shown.

inferred, as the light gray color in the TSP images indicative of laminar flow seems to extend downstream of the front in some regions (see for example from y = 0.4 m to 0.65 m in Fig. 4(c) for configuration III) or a dark gray color indicative of transitional or turbulent flow seems to be upstream of the extracted front (see for example from y = 0.8 m to 0.95 m in Fig. 4(d)). This concern was raised by Refs. [23, 49], who processed the TSP images to extract the transition front based on the temperature step method and a heating layer approach [50]. The uncertainty of the extracted fronts from the TSP images needs to be addressed to quantify the performance of the predicted transition fronts.

The mean flow solutions for the selected configurations are evaluated with the measured surface pressure coefficient, C_p, at the spanwise locations indicated in Fig. 5, where the pressure ports were arranged across the semispan CRM-NLF model. Figures 6 and 7 show the comparison of the measured and calculated pressure coefficients for the FT solution and the IT solution corresponding to the third iteration along rows A through H for configurations I and III, respectively. Similar results were found for configurations II and IV. A reasonable agreement is found between the CFD solutions and experimental measurements across the span of the wing. The suction peak level, the rapid acceleration near the leading edge, and the mild adverse pressure gradient in the midchord section of the upper surface are captured accurately. The pressure levels measured on the suction side of the wing appear to be slightly higher than that predicted by the computations, which was also observed by the computational results shown by Lynde et al. [19]. A significant difference in the location of the shocks is observed between the FT and IT solutions across the wing span for the three configurations. The shock location is generally in better agreement with the measurements for the FT computations, but the location is delayed in the IT solutions, which reflects a high level of viscous-inviscid interaction in the solutions. However, the pressure ports were deemed to trip the boundary layer and led to early laminar-turbulent transition along the corresponding span locations [18], which would explain the better agreement of the measured values with the FT simulation results.

IV. Summary and Concluding Remarks

The boundary-layer transition over the common research model with natural laminar flow (CRM-NLF) aircraft configuration is modeled with the dual N-factor method that accounts for the linear amplification of Tollmien-Schlichting (TS) waves and stationary crossflow (CF) waves. Flow conditions are selected to match those from a recent wind tunnel experiment in the National Transonic Facility at the NASA Langley Research Center [18–20]. The mean flow solutions are calculated with the OVERFLOW 2.3b solver as either a fully turbulent flow or as partly laminar flow with an imposed transition front on the surface of the wing along with the Spalart-Allmaras turbulence model in the turbulent portion of the flow. The proposed transition modeling method consists of an iterative procedure that begins with an initial transition front aligned with the most upstream shock from the fully turbulent solution and iteratively updates the

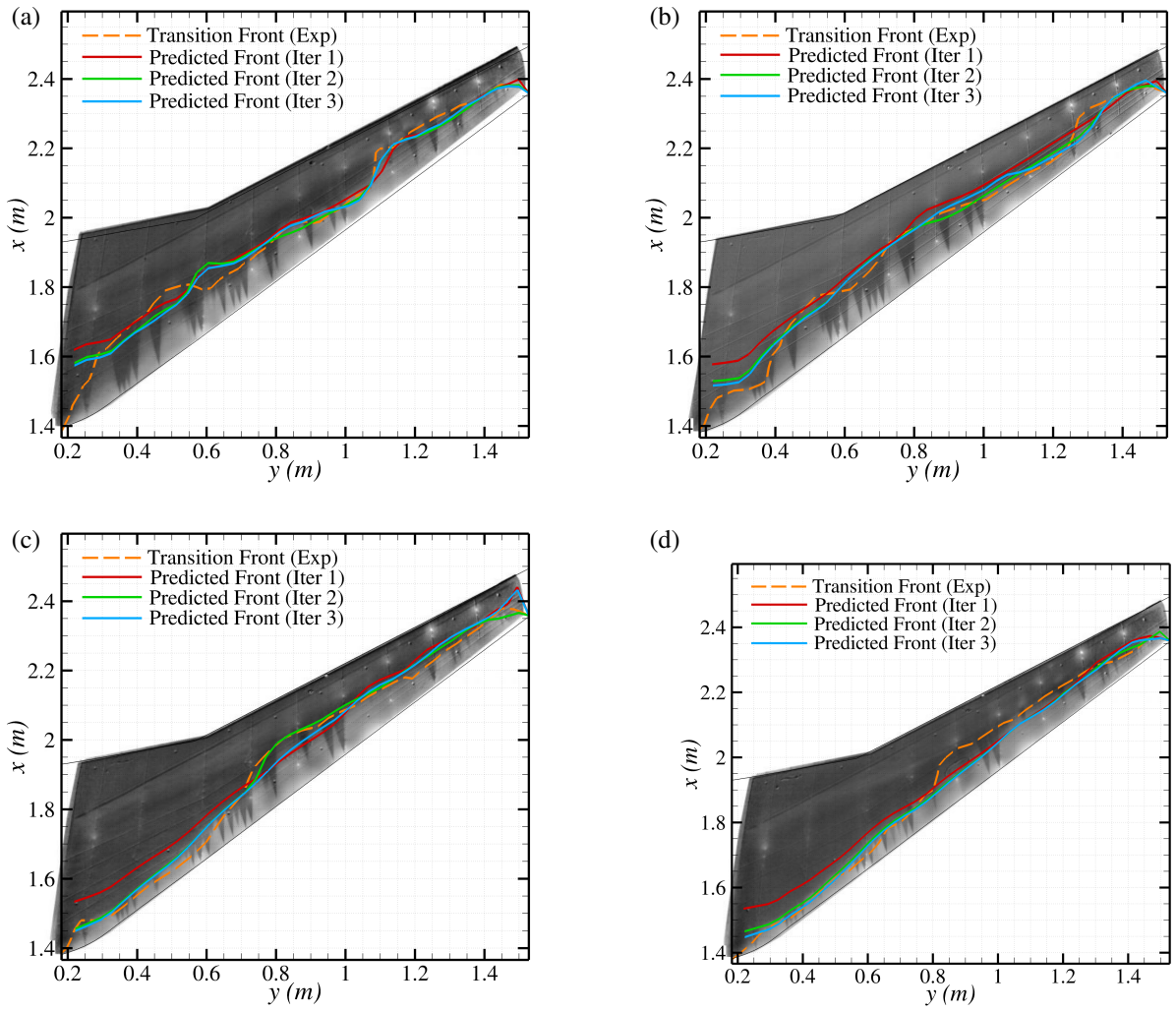


Fig. 4 Predicted transition locations using the dual $N_{TS} - N_{CF}$ criterion for three iterations over the TSP images shown along with experimental transition front for configurations (a) I, (b) II, (c) III, and (d) IV.

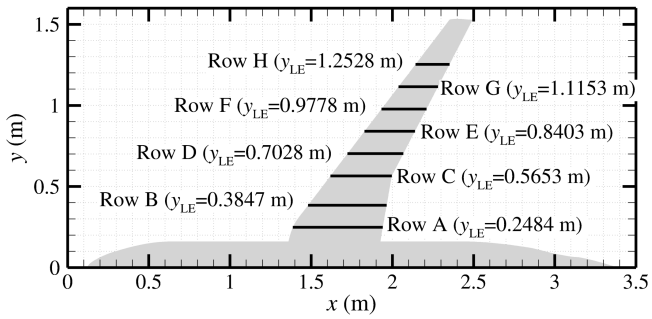


Fig. 5 Spanwise stations where the pressure ports were located in the CRM-NLF model.

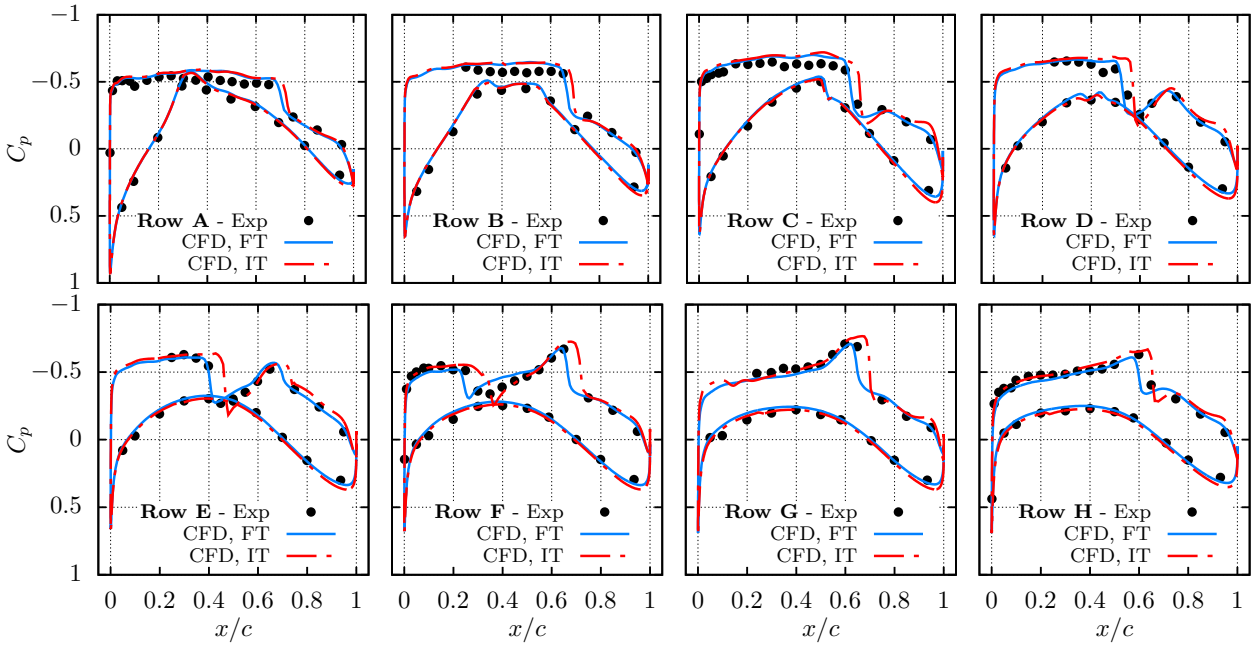


Fig. 6 Experimental and predicted pressure coefficient distributions at selected sections of the wing for configuration I ($AoA = 1.45°$). The solid lines correspond to the FT solution and the dash-dotted lines correspond to the IT solution corresponding to the third iteration.

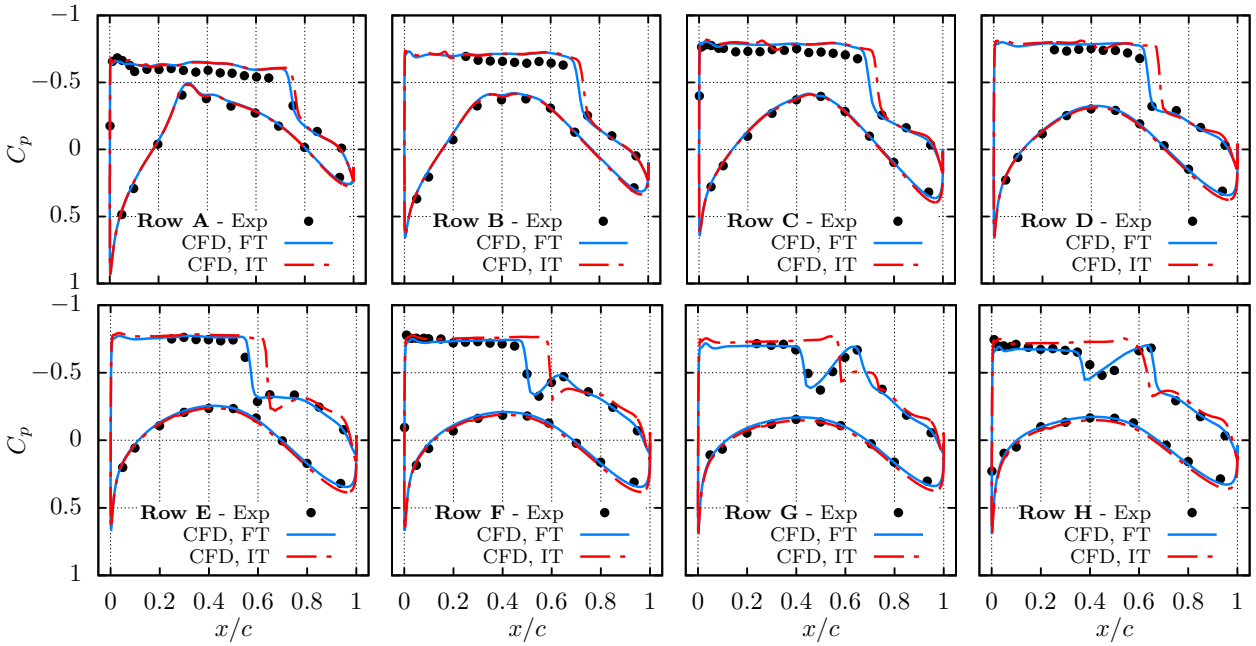


Fig. 7 Experimental and predicted pressure coefficient distributions at selected sections of the wing for configuration III ($AoA = 2.46°$). The solid lines correspond to the FT solution and the dash-dotted lines correspond to the IT solution corresponding to the third iteration.

imposed front with the predictions based on the dual N-factor criterion.

Results for the fully turbulent and imposed transition solutions are presented for $Re_{MAC} = 15\times10^6$ and $AoA = 1.45°$, 1.98°, 2.46°, and 2.94°. The dual $N_{TS} - N_{CF}$ criterion [35] is used to predict the transition front. The critical N_{CF} and N_{TS} are set equal to 6 based on prior analysis [26]. The predicted transition corresponds to the locus of chordwise locations where either the shock front has been reached or the indicator function for the dual N-factor criterion has reached unity. The results are presented for three iterations and show a favorable agreement with the experimental transition locations for all four angles of attack. The pressure coefficients are found to agree well with the measured values at the selected wingspan stations, although the imposed transition front solutions show a consistent downstream shift of the shock location with respect to the fully turbulent solutions and with respect to the experimental measurements. This shift indicates that the solution is sensitive to the effects of viscous-inviscid interaction, although the agreement with the measured surface pressures within the laminar region of the solution is not visually altered. During the experiments, the pressure ports were likely tripping the boundary layer and inducing an early transition along those spanwise stations [19] and that would explain the better agreement of the fully turbulent solution at those stations.

Additional computations to be reported in a future article are being performed to study the effect of the Reynolds number, as well as the effects of the surface curvature and nonparallel terms disregarded by the commonly used quasiparallel LST analysis. Also, there is some uncertainty concerning what truly represents the transition front based on the TSP images from the CRM-NLF experiment. An ongoing quantification of this uncertainty in the transition front should provide a more meaningful assessment of the computational models.

Acknowledgments

This research is sponsored by the NASA Transformational Tools and Technologies (TTT) project of the Transformative Aeronautics Concepts Program under the Aeronautics Research Mission Directorate. The first two authors' research is funded through the National Institute of Aerospace (NIA) under the cooperative agreement 2A00 (Activity 201133). The computational resources supporting this work were provided by the K cluster at NASA Langley Research Center and by the NASA High-End Computing (HEC) Program through the NASA Advanced Supercomputing (NAS) Division at the Ames Research Center.

References

[1] *Subsonic Fixed Wing Project Overview*, NASA FAP 2008 Annual Meeting, Atlanta, 2008.

[2] Report of the Group of Personalities, "European Aeronautics: A Vision for 2020," Europan Commission Rept. KI-34-01-827-EN-C, January 2001.

[3] Slotnick, J., Khodadoust, A., Alonso, J., Darmofal, D., Gropp, W., Lurie, E., and Mavriplis, D., "CFD Vision 2030 Study: A Path to Revolutionary Computational Aerosciences," Tech. Rep. CR-2014-218178, NASA, 2014.

[4] Medida, S., "Correlation-Based Transition Modeling for External Aerodynamic Flows," Ph.D. thesis, University of Maryland, 2014.

[5] Krumbein, A., Krimmelbein, N., Grabe, C., and Shengyang, N., "Development and Application of Transition Prediction Techniques in an Unstructured CFD Code (Invited)," AIAA Paper 2015-2476, 2015. doi:10.2514/6.2015-2476.

[6] Coder, J. G., "Further Development of the Amplification Factor Transport Transition Model for Aerodynamic Flows," AIAA Paper 2019-0039, Jan 2019. doi:10.2514/6.2019-0039.

[7] Smith, A. M. O., and Gamberoni, N., "Transition, Pressure Gradient and Stability Theory," Tech. Rep. ES-26388, Douglas Aircraft Division, 1956.

[8] Ingen, J. L. v., "A Suggested Semi-Empirical Method for the Calculation of the Boundary Layer Transition Region," *Technische Hogeschool Delft, Vliegtuigbouwkunde, Rapport VTH-74*, 1956.

[9] Herbert, T., "Parabolized Stability Equations," *Annual Review of Fluid Mechanics*, Vol. 29, No. 1, 1997, pp. 245–283. doi:10.1146/annurev.fluid.29.1.245.

[10] Campbell, R., Campbell, M., and Streit, T., "Progress Toward Efficient Laminar Flow Analysis and Design," AIAA Paper 2011-3527, 2011. doi:10.2514/6.2011-3527.

[11] Cliquet, J., Houdeville, R., and Arnal, D., "Application of Laminar-Turbulent Transition Criteria in Navier-Stokes Computations," *AIAA Journal*, Vol. 46, No. 5, 2008, pp. 1182–1190. doi:10.2514/1.30215.

[12] Davis, M. B., Reed, H., Youngren, H., Smith, B., and Bender, E., "Transition Prediction Method Review Summary for the Rapid Assessment Tool for Transition Prediction (RATTraP)," Tech. Rep. AFRL-VA-WP-TR-2005-3130, Lockheed Martin Corporation, June 2005.

[13] Drela, M., "Implicit Implementation of the Full E^N Transition Criterion," AIAA Paper 2003-4066, Jun 2003. doi:10.2514/6.2003-4066.

[14] Drela, M., and Giles, M. B., "Viscous-Inviscid Analysis of Transonic and Low Reynolds Number Airfoils," *AIAA Journal*, Vol. 25, No. 10, 1987, pp. 1347–1355. doi:10.2514/3.9789.

[15] Krumbein, A., Krimmelbein, N., and Grabe, C., "Streamline-Based Transition Prediction Techniques in an Unstructured Computational Fluid Dynamics Code," *AIAA Journal*, Vol. 55, No. 5, 2017, pp. 1548–1564. doi:10.2514/1.J054990.

[16] Krumbein, A. M., "Automatic Transition Prediction and Application to Three-Dimensional Wing Configurations," *Journal of Aircraft*, Vol. 44, No. 1, 2007, pp. 119–133. doi:10.2514/1.22254.

[17] Perraud, J., Arnal, D., Casalis, G., Archambaud, J.-P., and Donelli, R., "Automatic Transition Predictions using Simplified Methods," *AIAA Journal*, Vol. 47, No. 11, 2009, pp. 2676–2684. doi:10.2514/1.42990.

[18] Lynde, M. N., Campbell, R. L., Rivers, M. B., Viken, S. A., Chan, D. T., Watkins, A. N., and Goodliff, S. L., "Preliminary Results from an Experimental Assessment of a Natural Laminar Flow Design Method," AIAA Paper 2019-2298, 2019. doi:10.2514/6.2019-2298.

[19] Lynde, M. N., Campbell, R. L., and Viken, S. A., "Additional Findings from the Common Research Model Natural Laminar Flow Wind Tunnel Test," AIAA Paper 2019-3292, 2019. doi:10.2514/6.2019-3292.

[20] Rivers, M. B., Lynde, M. N., Campbell, R. L., Viken, S. A., Chan, D. T., Watkins, A. N., and Goodliff, S. L., "Experimental Investigation of the NASA Common Research Model with a Natural Laminar Flow Wing in the NASA Langley National Transonic Facility," AIAA Paper 2019–2189, 2019. doi:10.2514/6.2019-2189.

[21] Lynde, M. N., and Campbell, R. L., "Computational Design and Analysis of a Transonic Natural Laminar Flow Wing for a Wind Tunnel Model," AIAA Paper 2017-3058, 2017. doi:10.2514/6.2017-3058.

[22] Fischer, J., Soemarwoto, B., and van der Weide, E., "Automatic Transition Prediction in a Navier-Stokes Solver Using Linear Stability Theory," *AIAA Journal*, Vol. 59, No. 7, 2021, pp. 2409–2426. doi:10.2514/1.J059910.

[23] Krumbein, A., Francois, D., and Krimmelbein, N., "Transport-Based Transition Prediction for the Common Research Model Natural Laminar Flow Configuration," *Journal of Aircraft*, Vol. 59, No. 6, 2022, pp. 1562–1573. doi:10.2514/1.C036918.

[24] Krimmelbein, N., and Krumbein, A., "Transition Prediction for the NASA CRM-NLF with the E^N-Method using Incompressible and Compressible Linear Stability Analysis," AIAA Paper 2022-1953, 2022. doi:10.2514/6.2022-1953.

[25] Malik, M., Liao, W., Lee-Rausch, E., Li, F., Choudhari, M., and Chang, C.-L., "Computational Anaysis of the G-III Laminar Flow Glove," AIAA 2011-3525, 2011.

[26] Paredes, P., Paredes, P., Chouhdari, M., Li, F., Hildebrand, N., and Chang, C.-L., "Transition Analysis for the CRM-NLF Wind Tunnel Configuration," AIAA 2021-1431, 2021.

[27] Venkatachari, B., Paredes, P., Chouhdari, M., Li, F., and Chang, C.-L., "Transition Analysis for the CRM-NLF Wind Tunnel Configuration using Transport Equation Models and Linear Stability Correlations," AIAA 2022-1542, 2022.

[28] Halila, G., Chen, G., Shi, Y., Fidkowski, K., and Martins, J., "High-Reynolds Number Transitional Flow Prediction using a Coupled Discontinuous-Galerkin RANSPSE Framework," AIAA 2019-0974, 2019.

[29] Venkatachari, B., Carnes, J., Chang, C.-L., and Choudhari, M., "Boundary-Layer Transition Prediction Through Loose Coupling of OVERFLOW and LASTRAC," AIAA 2022-3682, 2022.

[30] Hildebrand, N., Chang, C.-L., Choudhari, M., Li, F., Nielsen, E., Venkatachari, B., and Paredes, P., "Coupling of the FUN3D Unstructured Flow Solver and the LASTRAC Stability Code to Model Transition," AIAA 2022-1952, 2022.

[31] Vogel, E., Venkatachari, B., Paredes, P., Li, F., and Choudhari, M., "CFD Integrated Transition Modeling for High-Speed Flows via Coupled OVERFLOW-LASTRAC Analysis," AIAA 2023-0438, 2023.

[32] Chang, C.-L., "LASTRAC.3d: Transition Prediction in 3D Boundary Layers," AIAA Paper 2004-2542, 2004.

[33] Chang, C.-L., "Langley Stability and Transition Analysis Code (LASTRAC) Version 1.2 User Manual," NASA TM-2004-213233, 2004.

[34] Horstmann, K., Redeker, G., Quast, A., Dressler, U., and Bieler, H., "Flight Test Wih a Natural Laminar Flow Glove on a Transport Aircraft," AIAA 90-3044, 1990.

[35] Arnal, D., "Boundary Layer Transition: Prediction Based on Linear Theory," *Special course on Progress in Transition Modeling. AGARD. R-793*, 1994, pp. 1–62.

[36] Schrauf, G., Perraud, J., Vitiello, D., and Lam, F., "Comparison of Boundary-Layer Transition Predictions Using Flight Test Data," *Journal of Aircraft*, Vol. 35, No. 6, 1998, pp. 891–897. doi:10.2514/2.2409.

[37] Crouch, J., Sutanto, M., Witkowski, D., Watkins, A., Rivers, M., and Campbell, R., "Assessment of the National Transition Facility for Natural Laminar Flow Testing," AIAA Paper 2010-1302, 2010. doi:10.2514/6.2010-1302.

[38] King, R., Andino, M., Melton, L., Eppink, J., and Kegerise, M., "Flow Disturbance Measruements in the NationalTransonicFacility," *AIAA Journal*, Vol. 52, No. 1, 2014, pp. 116–130. doi:10.2514/1.J052429.

[39] Jameson, A., Schmidt, W., and Turkel, E., "Numerical Solution of the Euler Equations by Finite Volume Methods using Runge Kutta Time Stepping Schemes," AIAA 1981-1259, 1981.

[40] Tramel, R., Nichols, R., and Buning, P., "Addition of Improved Shock-Capturing Schemes to OVERFLOW2.1," AIAA 2009-3988, 2009.

[41] Vassberg, J. C., DeHaan, M. A., Rivers, M. S., and Wahls, R. A., "Restrospective on the Common Research Model for Computational Fluid Dynamics Validation Studies," *Journal of Aircraft*, Vol. 55, No. 4, 2018, pp. 1325–1337. doi:10.2514/1.C034906.

[42] Campbell, R. L., and Lynde, M., "Expanding the Natural Laminar Flow Boundary for Supersonic Transports," AIAA Paper 2016-4327, 2016. doi:10.2514/6.2016-4327.

[43] Mack, L., "Transition Prediction and Linear Stability Theory," *Laminar-Turbulent Transition. AGARD. CP-224*, 1977, pp. 1.1–1.22.

[44] Nichols, H., and Buning, P., "User's Manual for OVERFLOW 2.3," , August 2019. URL `https://overflow.larc.nasa.gov/home/users-manual-for-overflow-2-3/`.

[45] Spalart, P., and Allmaras, S., "A One-Equation Turbulence Model for Aerodynamc Flows," *Recherche Aerospatiale*, Vol. 1, 1994, pp. 5–21.

[46] Roe, P. L., "Approximate Riemann Solvers, Parameter Vectors, and Difference Schemes," *Journal of Computational Physics*, Vol. 43, No. 2, 1981, pp. 357–372.

[47] Nichols, R., Tramel, R., and Buning, P., "Solver and Turbulence Model Upgrades to OVERFLOW 2 for Unsteady and High-Speed Applications," AIAA Paper 2006-2824, 2006. doi:10.2514/6.2006-2824.

[48] Venkatachari, B., Paredes, P., Derlaga, J., Buning, P., Chouhdari, M., Li, F., and Chang, C.-L., "Assessment and Improvement of RANS-Based Transition Models Based on Experimental Data of the Common Research Model with Natural Laminar Flow," AIAA 2021-1430, 2021.

[49] Krimmelbein, N., and Krumbein, A., "Determination of Critical N-Factors for the CRM-NLF Wing," *New Results in Numerical and Experimental Fluid Mechanics XIII*, edited by A. Dillmann, G. Heller, E. Krämer, and C. Wagner, Springer International Publishing, Cham, 2021, pp. 195–204. doi:10.1007/978-3-030-79561-0_19.

[50] Watkins, A., Goodman, K., and Peak, S., "Transition Detection at Cryogenic Temperatures using a Carbon-Based Resistive Heating Layer Coupled with Temperature Sensitive Paint," AIAA 2019-2191, 2019.